

## Dynamics of self-interstitial cluster migration in pure $\alpha$ -Fe and Fe-Cu alloys

J. Marian,<sup>1</sup> B. D. Wirth,<sup>1</sup> A. Caro,<sup>2</sup> B. Sadigh,<sup>1</sup> G. R. Odette,<sup>3</sup> J. M. Perlado,<sup>4</sup> and T. Diaz de la Rubia<sup>1</sup>

<sup>1</sup>*Chemistry and Materials Science Directorate, Lawrence Livermore National Laboratory, P.O. Box 808, L-353, Livermore, California 94550*

<sup>2</sup>*Instituto Balseiro, Centro Atómico Bariloche, 8400 Bariloche, Argentina*

<sup>3</sup>*Department of Mechanical and Environmental Engineering, University of California, Santa Barbara, California 93106*

<sup>4</sup>*Instituto de Fusión Nuclear, Universidad Politécnica de Madrid, C/José Gutiérrez Abascal, 2, 28006 Madrid, Spain*

(Received 1 November 2001; revised manuscript received 17 January 2002; published 21 March 2002)

We report the results of molecular dynamics simulations of self-interstitial cluster diffusion in pure  $\alpha$ -Fe and in a dilute Fe-1.0 at. % Cu alloy for a number of cluster sizes,  $n \leq 20$ . We find that the effect of this oversized substitutional solute is to enhance the three-dimensional character of small-cluster diffusion and to impact the general cluster diffusion properties. We explain this through a mechanism directly based on the interactions between the atomic displacement field of the Cu atoms and the self-interstitial clusters. Based on these results, we derive simple power laws for the extrapolation of migration energies and diffusion prefactors to larger sizes, required for longer-range microstructural evolution models. These laws represent an improvement over current parametrizations used in previous calculations.

DOI: 10.1103/PhysRevB.65.144102

PACS number(s): 61.72.Bb, 66.30.Fq, 61.82.Bg

### I. INTRODUCTION

The structure and mobility of self-interstitial atom (SIA) clusters has profound significance on the microstructural evolution of irradiated materials. Recent molecular dynamics (MD) simulations, both in bcc and fcc materials, show that such clusters form following the thermal spike stage of high-energy displacement cascades as a consequence of cooperative phenomena without long-range diffusion.<sup>1-3</sup> Diffuse x-ray scattering experiments at temperatures below stage I in neutron-irradiated Cu provide evidence to support these observations.<sup>4,5</sup> Transmission electron microscopy (TEM) analyses in other metals also confirm the formation of interstitial clusters following the collapse of displacement cascades.<sup>6,7</sup>

Since these studies of SIA cluster production in cascades, a number of authors have shown that the clusters develop into perfect dislocation loops with high mobility and execute one-dimensional migration.<sup>8-10</sup> A vast range of irradiation effects, which occur over very wide time scales, are mediated by the transport and ultimate fate of these cascade defects. The importance of understanding the production, mobility, and character of the SIA clusters has been emphasized by Trinkaus *et al.*<sup>11</sup> and has led to the development of dislocation- and production-bias theories to explain long-term damage accumulation and microstructural evolution in irradiated materials.<sup>12,13</sup> Other topics where SIA formation and diffusion are important include the absence of small, observable dislocation loops in ferritic materials in low-temperature, low-dose irradiation;<sup>14</sup> the source and mechanisms of point defect cluster hardening, including post-yield-strain hardening;<sup>15</sup> cluster-decorated dislocation structures;<sup>11</sup> and vacancy and interstitial sink strength and bias.<sup>16</sup>

Specifically, computer simulation has revealed that large clusters of interstitial atoms in  $\alpha$ -Fe form perfect dislocation loops with Burgers vector  $\mathbf{b} = \frac{1}{2}\langle 111 \rangle$  that have  $\{110\}$  habit planes and high one-dimensional mobility.<sup>8,10,17</sup> The MD studies show that small, strongly bound interstitial clusters

(two- to about five-SIA clusters) exhibit long-range, three-dimensional (3D) diffusion, which occurs by reorientation of the constituent  $\langle 111 \rangle$  dumbbells from one  $\langle 111 \rangle$  direction to another.<sup>8,17</sup> However, as cluster size increases, reorientation from one Burgers vector to another is increasingly more difficult to achieve and, at least during MD time scales, no 3D motion is observed even at the highest temperatures. At larger sizes, Wirth *et al.*<sup>8</sup> describe SIA clusters as perfect prismatic loops whose motion is governed by the propagation of intrinsic kinks originated at the periphery of the loops through a series of consecutive  $\{110\}$  planes. On the contrary, several studies suggest that the motion of the loops is the combination of independent, weakly correlated  $\langle 111 \rangle$  crowdion jumps.<sup>18</sup> However, to date, this work has all been carried out in pure systems, which ignores the strain field contributions of alloy additions on cascade evolution and defect transport. In this regard, aspects important to cluster formation, mobility, and growth, such as the effect of impurities or the interaction among loops, remain to be investigated.

One of the most widely studied problems in the nuclear industry is the lifetime extension of operating reactor pressure vessels (RPV's).<sup>19-21</sup> It is known that both Cu precipitates and ultrafine matrix nanofeatures (neutron-irradiation-induced point defect clusters) are responsible for hardening in RPV steels and could limit operational lifetime. In this paper, we report on SIA cluster migration in a dilute ( $\sim 1.0$  at. %, similar to RPV steels) Fe-Cu binary alloy within the framework of defect diffusion in multicomponent systems. We attempt to isolate the effect of oversized, substitutional Cu atoms upon SIA cluster motion with the objective of developing a more complete understanding of the physics and mechanisms involved in the interaction among Cu impurity atoms and interstitial defects. Based on this we derive general laws for the diffusion parameters (migration energies and prefactors) as a function of cluster size in both pure Fe and the Fe-Cu alloy, required to generate the necessary data as input into longer-range Monte Carlo or rate theory models.

While Cu atoms do not have a significant impact on primary damage production in dilute Fe-Cu alloys,<sup>22</sup> they do have a noticeable influence on defect transport properties. Marian and co-workers<sup>23</sup> have shown that Cu atoms perturb the rate of solvent jumps occurring in their vicinity and attract vacancies so as to effectively increase the neighboring vacancy concentration. Self-interstitial atom diffusion is also affected by the Cu in solution. Based on atomic displacement field interactions, Marian *et al.*<sup>24</sup> have shown that Cu atoms change the configuration-dependent energies of nearby SIA's, resulting in a decreased effective activation energy for SIA migration and a reduced diffusion prefactor. In this paper we extend the calculations to determine the effect of oversized solutes on the diffusion of larger interstitial clusters in bcc Fe.

## II. COMPUTATIONAL MODEL

We have performed calculations for 1-, 2-, 3-, 6-, 10-, 15-, and 20-SIA clusters both in pure  $\alpha$ -Fe and Fe-1.0 at. % Cu. All MD simulations have been carried out with the MDCASK code<sup>25</sup> using the Fe-Cu many-body interatomic potential of Ackland and co-workers.<sup>26</sup> Calculations were made at temperatures ranging between 400 and 1300 K. For the Fe-Cu cases, Cu atoms were randomly distributed over the simulation box up to the desired proportion (1.0 at. %). The self-interstitial atoms were identified by analyzing all Wigner-Seitz cells of the corresponding perfect lattice, the criterion adopted for interstitial identification being the existence of more than one atom in the same cell.

For the study of cluster migration it is difficult to establish the discreteness of a diffusive jump since many individual  $\langle 111 \rangle$  motions of the crowdions forming part of a cluster can occur without necessarily producing net cluster diffusion. These jumps are merely vibrational excursions of the individual SIA's about the equilibrium lattice positions. Moreover, it is possible for an individual SIA to perform several jumps away from the compact cluster structure. The number of such jumps increases with temperature, although on average the cluster keeps its compact configuration. However, we have observed by visual examination that the individual interstitials most likely to undergo such independent jumps are those at or close to the corners of the loops. As observed previously by Wirth *et al.*, these defects can trigger the nucleation of an intrinsic kink, which, upon propagation along the contour of the cluster, can produce a collective translation resulting in effective overall diffusion.<sup>8</sup> Therefore, to calculate cluster diffusivities we have used a method that relies on the movement of the center of mass of the cluster based on its total mean-square displacement of travel.

Following the procedure described by Guinan *et al.*,<sup>27</sup> we have calculated the diffusion coefficient of each cluster,  $I_n$  ( $n$ , number of interstitials in the cluster),  $D_n$ , in both pure Fe and the Fe-Cu alloy. Because of the highly correlated nature of interstitial diffusion, long runs are required to warrant numerical convergence. For that reason, cluster migration was monitored during times ranging from 0.3 to 1.2 ns, depending on temperature and cluster size. Each run is then divided into an arbitrary number  $m$  of time segments and the

mean-square displacement of the cluster's center of mass,  $\langle R^2 \rangle$ , was measured. We define  $D_n$  as

$$D_n = \frac{1}{m} \sum_{i=1}^m \frac{\langle R^2 \rangle}{2n_d t_i} = \frac{1}{m} \sum_{i=1}^m D_{ni}; \quad (1)$$

i.e., the cluster diffusivity is the average of all the  $D_{ni}$  values calculated in each segment  $i$ , where  $n_d$  is the dimensionality of the motion (1, 2, or 3) and  $t_i$  the corresponding segment time length (the minimum  $t_i$  was chosen to be 50 ps, high enough to contain several self-interstitial jumps). Prior to computing  $D_n$ , however, every  $I_n$  trajectory was visually analyzed to determine  $n_d$ . Of course, the accessible time duration of MD simulations may not be long enough to unequivocally establish the 3D or 1D character of cluster migration, but it gives an idea about the long-term diffusional character of the cluster. From the results at each temperature, a least-squares, exponential fit of the data was then used to evaluate the migration energy  $E_m$  and the frequency factor  $D_0$  from the Arrhenius diagram. Computation box sizes, simulated times, and dimensionality of cluster motion for each  $I_n$  are provided in Table I.

Prior to every microcanonical MD run at each selected temperature, we first determined the minimum-energy configuration of each cluster by way of low-temperature ( $\sim 10$  K) annealings for 10 ps followed by numerical quenching. Subsequently, the temperature was raised to its target value and the computational cell equilibrated for 10 additional ps. Finally, while the boundary between dislocation loop and interstitial cluster behavior is not completely clear from the atomistic point of view, in this work we use both terms interchangeably for the sake of convenience.

## III. RESULTS AND DISCUSSION

Diffusion coefficients along with the associated error bars for the interstitial clusters in pure Fe and the Fe-Cu alloy are plotted in Fig. 1 as a function of inverse temperature. Arrhenius behavior is observed throughout the whole temperature range for all clusters. The differences between the SIA diffusion coefficients in  $\alpha$ -Fe compared to Fe-1.0 at. % Cu are small, but notable, especially since the variation in  $D_0$  and  $E_m$  is greater than the statistical variance of the calculated diffusivities (of the order of 10%). This shows a clear, albeit relatively small, influence of Cu on the mechanisms that affect interstitial cluster migration.

It is important to note that Cu is an oversized substitutional solute in  $\alpha$ -Fe and, therefore, acts as a dilational center in the  $\alpha$ -Fe lattice. This local compressive strain is spherically symmetric and, in the bcc Fe crystal structure, produces a volume expansion of  $\Delta V \sim 0.3\%$  and  $\Delta V \sim 1.8\%$  in the first- (1 NN) and second-nearest-neighbor (2 NN) shells, respectively, and is negligible at farther distances.<sup>24</sup> On the other hand, the displacement (strain) field of the SIA clusters results from the linear combination of the individual  $\langle 111 \rangle$  crowdion strain fields, which are mainly of compressive nature (note, for the potentials employed here, that there is only one possible positively bound SIA-Cu complex when the SIA is in the form of a  $\langle 111 \rangle$  crowdion).<sup>24,26</sup> Therefore, the

TABLE I. Calculation and diffusion parameters (prefactors and migration energies) for all the studied clusters. The box size is given in lattice units, where  $a_0=2.87 \text{ \AA}$ . The dimensionality of the cluster motion,  $n_d$  (3D or 1D), indicated here is that observed during the limited MD time scales.

Cluster size ( $n$ )	Box size ( $a_0$ )	Simulation time (ns)	$n_d$	$D_o$ ( $\text{cm}^2 \text{ s}^{-1}$ )		$E_m$ (eV)	
				$\alpha\text{-Fe}$	Fe-1.0 at. % Cu	$\alpha\text{-Fe}$	Fe-1.0 at. % Cu
1	10	1.0	3	$1.94 \times 10^{-3}$	$1.15 \times 10^{-3}$	0.127	0.090
2	10	1.2	3	$1.48 \times 10^{-3}$	$1.15 \times 10^{-3}$	0.084	0.053
3	20	0.6	3 <sup>a</sup>	$1.42 \times 10^{-3}$	$5.50 \times 10^{-4}$	0.074	0.036
6	20	0.6	1	$3.02 \times 10^{-3}$	$1.60 \times 10^{-3}$	0.075	0.067
10	30	0.3	1	$2.70 \times 10^{-3}$	$1.50 \times 10^{-3}$	0.060	0.063
15	30	0.3	1	$1.17 \times 10^{-3}$	$7.01 \times 10^{-4}$	0.061	0.050
20	30	0.3	1	$1.27 \times 10^{-3}$	$3.59 \times 10^{-4}$	0.057	0.053

<sup>a</sup>In pure Fe, a one-dimensional random walk was observed for the three lowest temperatures (400, 575, and 750 K), whereas 3D motion was seen at 1000 K. In Fe-1.0 at. % Cu, 1D motion was observed at 500 K; at 800 K, one change in direction was recorded (2D motion); finally, at 1000 and 1200 K, 3D motion occurs. This has been properly accounted for in each case when computing the diffusion coefficient from Eq. (1).

effect of Cu solute atoms on SIA cluster migration can be rationalized using atomic displacement field interaction considerations. The Cu produces a decrease in both the prefactor and the migration energy for the  $I_1$ ,  $I_2$ , and  $I_3$ , whereas for larger clusters ( $I_6$ ,  $I_{10}$ ,  $I_{15}$ , and  $I_{20}$ ), which migrate only one dimensionally during the simulations, only a decrease in  $D_0$  is observed while the slope ( $E_m$ ) of the curves remains virtually constant. The factors responsible for these differences are separately addressed for migration energies and diffusion preexponential factors in Secs. III A and III B, respectively.

Another important aspect about cluster migration is the global migration mechanism of large loops. Visual analysis at the lowest temperatures for the  $I_{15}$  and  $I_{20}$  (400 K) reveals that random crowdion jumps outside the global habit plane of the cluster are more likely to occur at the loop corners. After several attempts of this kind, one of these jumps may be followed by several other crowdions, triggering the local nucleation of a *proto* kink that propagates around the periphery of the loop. When the kink completes the entire loop perimeter or encounters another kink, the process halts, the overall effect being a large collective motion of a portion of the cluster. Moreover, the nucleation of kinks is not completely random, but seems to follow a pattern so as to rotate the overall habit plane of the loop from  $\{110\}$  to pure-edge,  $\{111\}$  planes, as corresponds to a perfect, prismatic dislocation loop. This is in good agreement with the kink nucleation-propagation model of Wirth *et al.*<sup>8</sup> for large SIA loops using a slightly different Finnis-Sinclair potential.

### A. Effect on migration energy

The migration energies derived from the fitted exponential functions are compiled in Table I and plotted in Fig. 2. Notably, the clusters with an altered migration energy in the Fe-Cu alloy are those that exhibit 3D motion (Table I). Irrespective of their size, all  $\frac{1}{2}\langle 111 \rangle$  clusters in  $\alpha\text{-Fe}$  migrate one dimensionally along the direction of their Burgers vector. However, the overall migration behavior of small SIA clus-

ters results from rotations between differently oriented  $\langle 111 \rangle$  configurations and is, thus, three dimensional. This also holds true for single interstitials ( $I_1$ ), whose migration mechanism is a multiple-step process that involves rotations between the  $\langle 110 \rangle$ - and  $\langle 111 \rangle$ -oriented split dumbbell configurations, with no net motion associated, and one-dimensional translations along the  $\langle 111 \rangle$  directions through a series of crowdion jumps.<sup>28</sup> In a previous paper, we showed that the influence of oversized, substitutional Cu atoms on nearby  $I_1$ 's is to change the configuration-dependent energies as a result of atomic strain field interactions.<sup>24</sup> The altered SIA energies result in an enhanced rotation between the  $\langle 110 \rangle$  and  $\langle 111 \rangle$  configurations and a decreased effective activation energy for migration from approximately 0.13 to 0.09 eV. These arguments can be equally applied to the small, 3D migrating clusters studied here, although the intrinsic, minimum-energy configuration of these small 3D clusters is a set of strongly bound  $\langle 111 \rangle$  crowdions or dumbbells, rather than the  $\langle 110 \rangle$  dumbbell as for the  $I_1$ .

Therefore, in a like manner, the migration mechanism of di- or tri-interstitials is the combination of a rotation step from one  $\langle 111 \rangle$  configuration to another, plus a series of rapid, correlated  $\langle 111 \rangle$  jumps. When a  $I_2$  or  $I_3$  forms a negatively bound Cu-SIA cluster complex during its diffusion throughout the crystal lattice, the rotation tendency of the cluster is enhanced so that the compressive displacement field of the Cu atom can be more favorably accommodated to that of the interstitial cluster. This effect results in a decreased activation energy for direction change and, hence, in a reduced effective migration energy obtained from our MD simulations. Figure 3 shows a  $I_2$  rotation from a negative-binding-energy configuration ( $E_b = -0.13$  eV) to an almost neutral (slightly negatively bound) one ( $E_b = -0.03$  eV) at 600 K. In configuration (a), the di-interstitial is forced to stop by negative strain-field interactions with the Cu atom and, from there, (b), the cluster rearranges itself into a metastable structure in which the compressive region of the Cu atom's displacement field is better accommodated within the limited

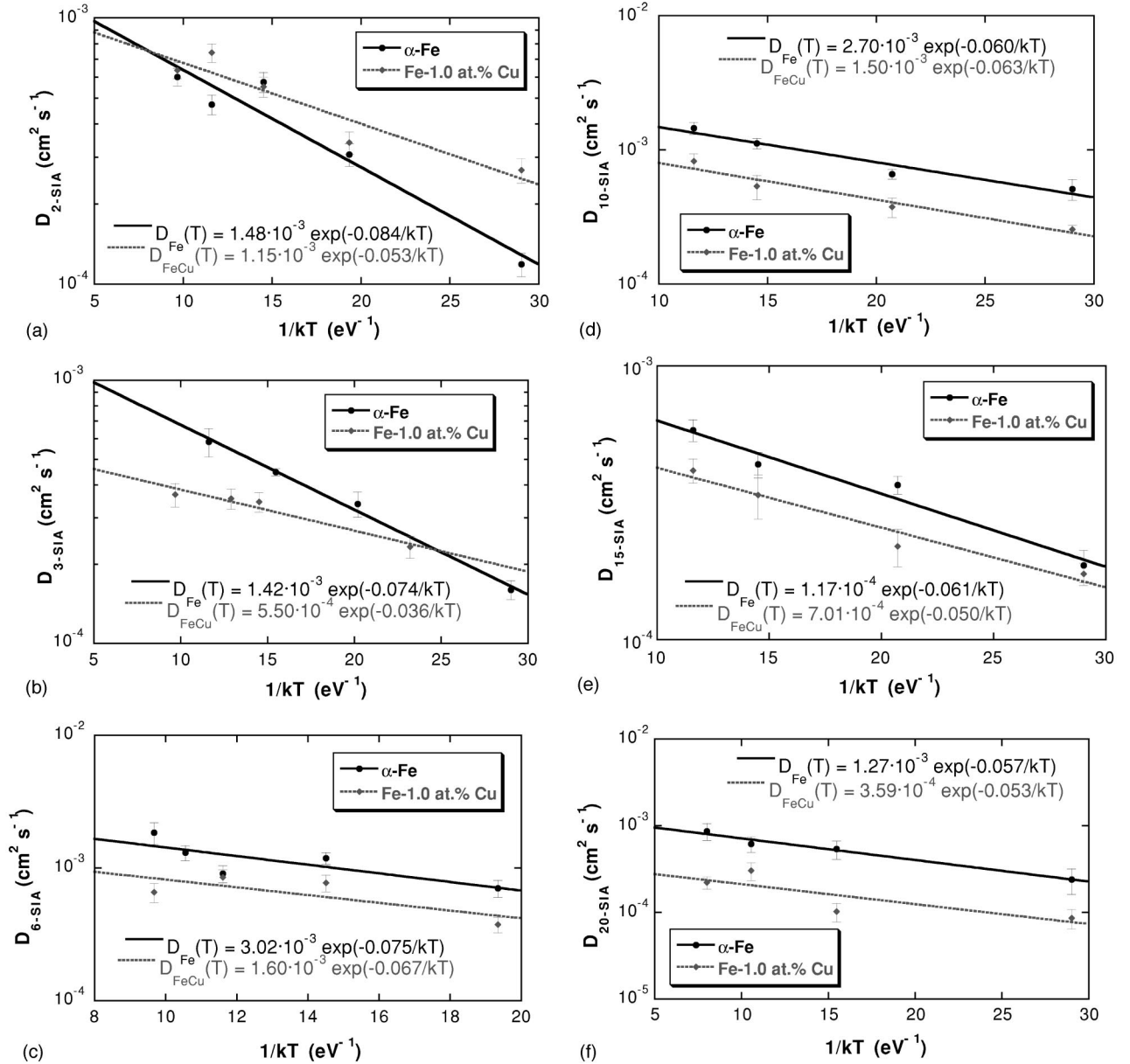


FIG. 1. Arrhenius plots of (a) 2-SIA, (b) 3-SIA, (c) 6-SIA, (d) 10-SIA, (e) 15-SIA, and (f) 20-SIA cluster diffusion coefficients in Fe and Fe–1.0 at. % Cu with their associated error bars. The data for the single interstitial are given in Ref. 24.

tensile region of the  $I_2$ . This effectively enhances the 3D character of single SIA's and small clusters. In this regard, analysis of the effective correlation factor, defined as  $f = D_t/D_n$ , where  $D_t$  is the tracer diffusion coefficient,<sup>29</sup> supports this conclusion. Averaging  $f$  over the temperature range of 560–1000 K for  $n=1$  (single SIA) and 400–1200 K for  $n=2$  (di-interstitial) resulted in values of 0.19 and 0.11, respectively, for pure Fe versus slightly higher (less correlated, more random diffusion) values of 0.24 and 0.13 for the Fe–1.0 at. % Cu alloy.

Due to the limited MD simulation times, it is sometimes difficult to establish the dimensionality of small cluster migration. Several workers have proposed  $n>3$  as the turning point from 3D to 1D diffusion based on cluster geometries and stacking-fault energy considerations,<sup>17,18</sup> but even for the

$I_3$  the change in migration direction occurs rather infrequently in either Fe or Fe-Cu and in our simulations it has only been observed at the highest two temperatures of 1000 and 1250 K (and one isolated case at 750 K in Fe-Cu). However, at these high temperatures, the effect of Cu is clearly appreciated in the form of more numerous, shorter  $\langle 111 \rangle$  trajectories giving rise to a more erratic migration. A comparison of  $I_3$  center-of-mass trajectories over 0.6 ns of time at 1000 K is shown in Fig. 4 and reveals the solute-enhanced 3D nature of the tri-interstitial diffusion in Fe-Cu. Further, at 750 K after 600 ps, one change in direction occurred for the  $I_3$  in Fe-Cu, whereas, under the same conditions in pure Fe, the  $I_3$  performed a perfect, 1D random-walk trajectory. While the statistical variance derived from having just one direction-change event is rather large and quantitatively in-



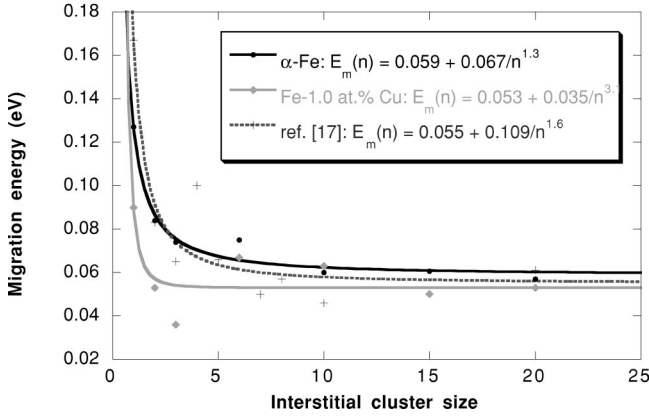


FIG. 2. Interstitial cluster migration energy barriers as a function of cluster size. The data obtained by Soneda and Díaz de la Rubia in pure Fe (Ref. 17) are shown for comparison. The tendency in Fe-Cu is to approach its asymptotic value faster than in pure Fe.

conclusive, it appears clear that the Cu in solution assists the rotation of these small clusters.

On the other hand, the larger simulated clusters ( $I_6$ ,  $I_{10}$ ,  $I_{15}$ , and  $I_{20}$ ) are seen to execute fully one-dimensional random walks without directional changes during molecular dynamics time scales, both in pure Fe and in the Fe-Cu alloy. Hence there is no dynamic basis for an activation energy reduction and the migration energies of these loops are very similar in both pure  $\alpha$ -Fe and Fe-1.0 at. % Cu (Table I).

The migration energy as a function of size is plotted in Fig. 2. Following Soneda and Díaz de la Rubia,<sup>17</sup> here we derive a simple general law of the form [ $E_m(n) = a + b/n^c$ ] in Fe and in Fe-1.0 at. % Cu to account for the decreased mobility of SIA clusters with increasing  $n$ , where  $a$ ,  $b$ , and  $c$  are constants. The physical meaning of  $a$  and  $c$  derives from dislocation theory.  $a$  represents the asymptotic migration energy value, related to the kink-pair nucleation energy (roughly constant in edge-type dislocations and large dislocation loops) and, from a smaller-cluster, phenomenological point of view, to the size-independent  $\langle 111 \rangle$  migration step. The exponent  $c$  gives an idea on how fast that value is approached, although the scaling law of  $E_m$  with  $n$  is not clear, and  $c$  may simply indicate the relative importance of the rotation component (present for small clusters) in the overall migration energy. The fitted functions are displayed in the

legend of Fig. 2. Two points are important to emphasize. First, regardless of the material, the migration energy tends to saturate for clusters with  $n > 6$  at a value of 0.05–0.06 eV (0.059 eV for pure Fe and 0.053 eV for Fe-Cu), which, as just mentioned, is an effective 1D migration energy barrier. Second, the asymptotic value is more rapidly approached in Fe-Cu ( $c = 3.1$ ) than in pure Fe ( $c = 1.3$ ); i.e., there is a weaker size dependence for cluster diffusion in the Fe-Cu system. Our results for pure Fe agree well with the analysis of Soneda and Díaz de la Rubia in Fe using a different embedded-atom model (EAM) potential<sup>17</sup> (Fig. 2).

## B. Diffusion prefactors

The diffusion prefactors extracted from the exponential functions of Fig. 1 are provided in Table I and plotted in Fig. 5. The data of Soneda and Díaz de la Rubia<sup>17</sup> is also shown for comparison. While these workers proposed a fit to the data of the same form as for the migration energy [ $D_0(n) = a + b/n^c$ ], SIA-cluster diffusion prefactors, unlike migration energies, do not saturate for large cluster sizes. This is because the cluster diffusivity should approach zero as the loop grows into a network dislocation, which does not move by thermal activation in the absence of an applied stress;<sup>30</sup> i.e., there is no saturation term for the dependence of  $D_0$  with  $n$ . Below follows a brief derivation of the scaling law of  $D_0$  with  $n$ .

In general, the time needed for the motion of kinks to produce a net cluster displacement,  $\tau_k$ , increases with increasing cluster perimeter  $L$  as kinks must propagate along the entire loop outline to displace it by one Burgers vector along the glide direction. If we consider this motion to be diffusive in nature (as the propagation of a kink pair along an infinitely long straight dislocation segment), then  $\tau_k \propto L^2$ . If, instead, we consider that, among other things, cluster size, loop curvature, and image forces induce stresses that influence kink motion, then  $\tau_k \propto L$ .<sup>31</sup> The real situation may be an intermediate combination between these two, with a *mechanically* biased (rather than purely thermally activated) diffusion mechanism that scales as  $L^S$ , with  $1 < S < 2$ . Here  $S$  is of course size dependent and will approach 2 as the cluster size increases and scale effects become less important. Since we are considering planar SIA clusters,  $L$  must scale with cluster size  $n$  as  $L \propto n^{1/2}$ , and since cluster diffusivity scales as  $\tau_k^{-1}$ , we have that  $D_0(n) \propto n^{-S/2}$ . Hence the diffusion

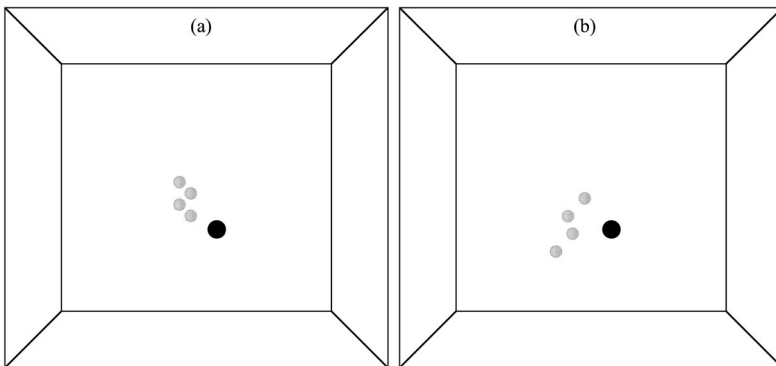


FIG. 3. Snapshots of the solute-driven rotation of a di-interstitial. In (a) the di-interstitial encounters a Cu atom along its  $\langle 111 \rangle$  trajectory. Due to the repulsive interaction, the defect rotates so as to minimize the intensity of the compressive atomic displacement field (b) and ready to resume its migration away from the solute atom.

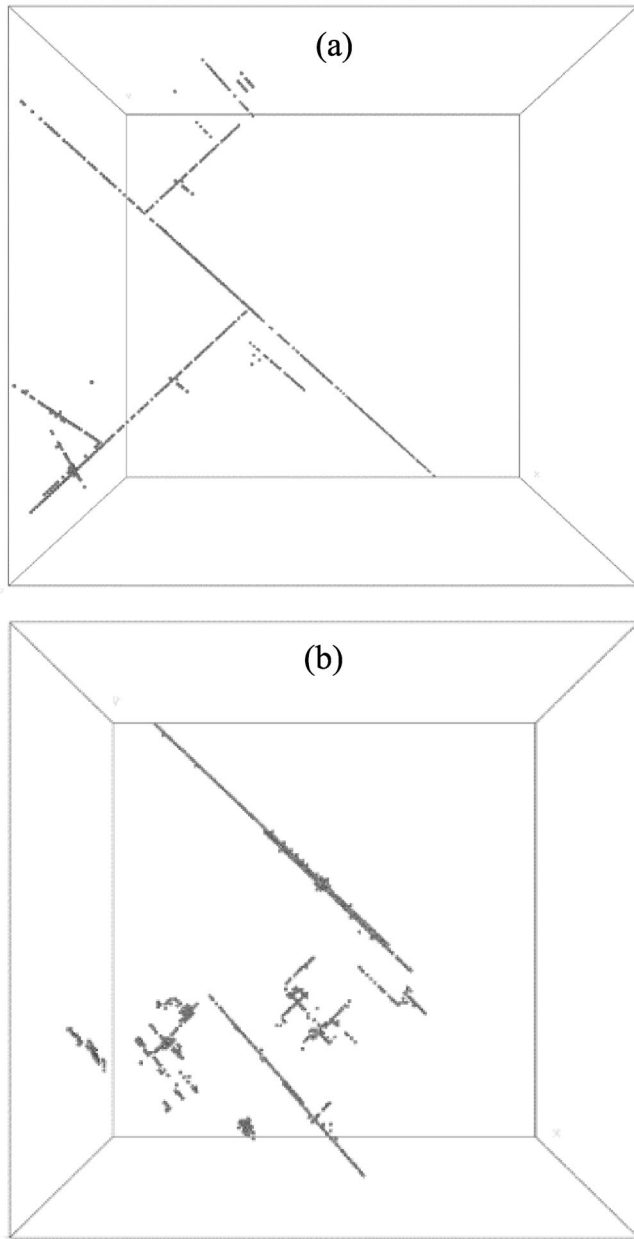


FIG. 4. Comparison of the three-dimensional trajectories of a three-SIA cluster in pure  $\alpha$ -Fe (a) and Fe-1.0 at. % Cu (b) at 1000 K. The trajectory in Fe contains longer  $\langle 111 \rangle$  segments and fewer direction changes than in Fe-Cu.

prefactor decreases monotonically with cluster size, and here we use simple expressions of the form  $D_0(n) = an^{-S/2}$  in both pure Fe and Fe-1.0 at. % Cu.

However, the curves of Fig. 5 for Fe and Fe-Cu show an initial decrease at low  $n$ 's, followed by a marked increase that gradually decays for large  $n$ 's. This is simply a numerical artifact that results from suddenly changing  $n_d$  in Eq. (1) from 3 to 1 due to the observed change in cluster motion dimensionality. It is expected, however, that, as 3D motion extends to larger sizes (by lengthening the simulation time scales), the abrupt transition observed will gradually smoothen. Interestingly, Soneda and Díaz de la Rubia did not observe such a transition, since they did not consider 1D

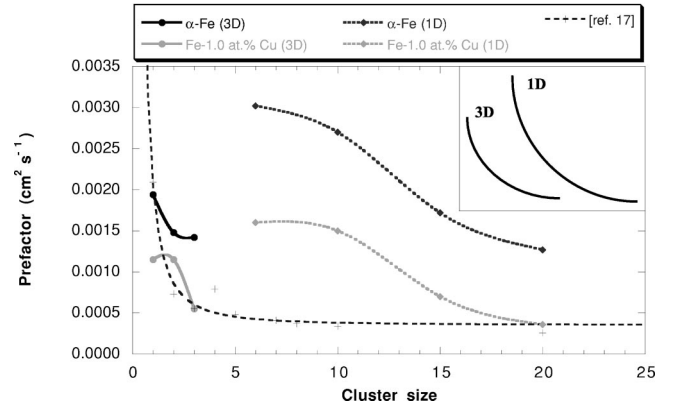


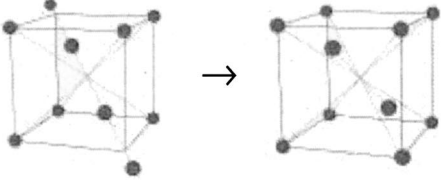
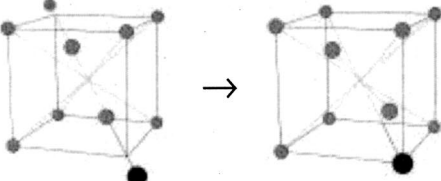
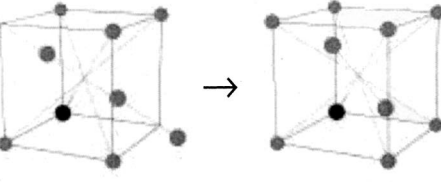
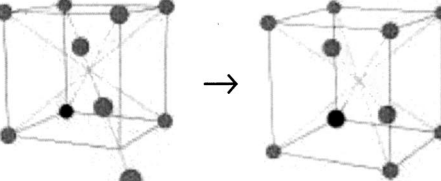
FIG. 5. Interstitial cluster diffusion pre-factors as a function of cluster size. The curves for both diffusion in pure Fe and Fe-1.0 at. % Cu clearly contain two parts (schematically represented in the inset), one corresponding to 3D and the other to 1D migration. Both curves are qualitatively similar, although the quantitative difference amounts to  $\sim 2.0$ . The data of Soneda and Díaz de la Rubia in pure Fe (Ref. 17) are shown for comparison.

motion for the numerical calculation of the diffusion coefficients. The inset in Fig. 5 shows schematically the twofold form of the curves where the 3D-1D transition may be shifted to larger cluster sizes as the time scale increases and 3D motion is observed for larger  $n$ . Nevertheless, we obtain a good fit to the 1D prefactor data with  $D_0(n) = 8.98 \times 10^{-3} n^{-0.61} \text{ (cm}^2 \text{ s}^{-1}\text{)}$  in pure Fe and  $D_0(n) = 5.07 \times 10^{-3} n^{-0.74} \text{ (cm}^2 \text{ s}^{-1}\text{)}$  in Fe-Cu. In their numerical study of SIA cluster migration in Fe, Barashev *et al.*<sup>18</sup> obtained a size dependence of the form  $n^{-0.7}$  using long-range pair potentials, in good agreement with our results. Albeit from the statistics derived from the calculations is difficult to extract definite conclusions, it appears as if solute atoms softened the stress field that biases the motion of kinks, making it more diffusive.

The diffusion prefactors for 1D motion in pure Fe are roughly 2 times those in Fe-1.0 at. % Cu and differ substantially from those calculated by Soneda Díaz de la Rubia.<sup>17</sup> The differences between the prefactor in pure Fe and in Fe-Cu arise from the fact that Cu atoms appear to reduce the average segment jump length of  $\langle 111 \rangle$  cluster translation jumps. This is a consequence of having a smaller attempt frequency, which is the dominant contribution to the pre-exponential factor. Any transition attempt frequency hinges on the vibrational states of the system at the equilibrium and saddle point configurations. Next, we derive a simple formulation that allows us to express the differences between the prefactors in Fe and Fe-Cu in terms of these vibrational properties.

For 3D migrating clusters, the average segment length  $l$  is proportional to the square root of the average number of jumps along the  $\langle 111 \rangle$  direction, which is in turn proportional to the time that the interstitial resides in the  $\langle 111 \rangle$  configuration,  $\tau_{\langle 111 \rangle}$ . This time of residence is proportional to the ratio of the probability for undergoing  $\langle 111 \rangle$  jumps and the probability to rotate out of the  $\langle 111 \rangle$  configuration into the  $\langle 110 \rangle$ :

TABLE II. Attempt frequencies and static energy barriers for first-nearest neighbor,  $\langle 111 \rangle$ -to- $\langle 110 \rangle$  (librational) transitions for the single interstitial in pure Fe (first row) and different mixed Cu-SIA structures. Only one elementary bcc cell is shown. Fe atoms are displayed in light gray and Cu atoms in black.

$\langle 110 \rangle$ - $\langle 111 \rangle$ transition	Attempt frequency (THz)	Static energy barrier (eV)
	9.96	0.12
	9.86	0.10
	9.92	0.10
	10.30	0.11

$$l^2 \propto \tau_{\langle 111 \rangle} \propto \frac{P(\langle 111 \rangle - \langle 111 \rangle)}{P(\langle 111 \rangle - \langle 110 \rangle)}, \quad (2)$$

where  $P$  is the probability of undergoing each transition. In our approach, these probabilities are the diffusivities in each case, i.e.,

$$P = \Gamma_0 \exp\left(-\frac{E_m}{kT}\right), \quad (3)$$

$$l^2 \propto \frac{\Gamma_0^{\langle 111 \rangle - \langle 111 \rangle} \exp\left(-\frac{E_m^{\langle 111 \rangle - \langle 111 \rangle}}{kT}\right)}{\Gamma_0^{\langle 111 \rangle - \langle 110 \rangle} \exp\left(-\frac{E_m^{\langle 111 \rangle - \langle 110 \rangle}}{kT}\right)}, \quad (4)$$

where  $\Gamma_0$  is the attempt frequency or prefactor. Then, since for diffusive processes  $D$  scales with  $l^2$ , according to our MD results we must have that, roughly,  $l_{\text{Fe}}^2/l_{\text{FeCu}}^2 \approx 2$ , i.e.,

$$\frac{l_{\text{Fe}}^2}{l_{\text{FeCu}}^2} \propto \frac{\frac{\Gamma_{0,\text{Fe}}^{\langle 111 \rangle - \langle 111 \rangle}}{\Gamma_{0,\text{FeCu}}^{\langle 111 \rangle - \langle 111 \rangle}} \exp\left(-\frac{E_{m,\text{Fe}}^{\langle 111 \rangle - \langle 111 \rangle} - E_{m,\text{Fe,Cu}}^{\langle 111 \rangle - \langle 111 \rangle}}{kT}\right)}{\frac{\Gamma_{0,\text{Fe}}^{\langle 111 \rangle - \langle 110 \rangle}}{\Gamma_{0,\text{FeCu}}^{\langle 111 \rangle - \langle 110 \rangle}} \exp\left(-\frac{E_{m,\text{Fe}}^{\langle 111 \rangle - \langle 110 \rangle} - E_{m,\text{Fe,Cu}}^{\langle 111 \rangle - \langle 110 \rangle}}{kT}\right)} \approx 2. \quad (5)$$

That is, in order to estimate the average jump length in each case, one needs to calculate the corresponding  $\Gamma_0$ 's and  $E_m$ 's.

In the harmonic approximation, the preexponential part or jump frequency of a system containing  $N$  atoms is given by

$$\Gamma_0 = \frac{\prod_i^{3N} \nu_i}{\prod_i \nu'_i}, \quad (6)$$

where the product extends over the total number of degrees of freedom of the system and  $\nu_i$  and  $\nu_i'$  are the frequencies of the normal modes in the equilibrium and saddle point configurations, respectively. The difference in energy between these two configurations yields the static migration energy barrier. In the subsections that follow we focus first on single SIA's, including simple Cu-SIA structures, to acquire a better understanding of the phonon modes created by single-interstitial defects and isolate their basic vibrational properties. Then, we incorporate this knowledge to analyze and compare a more complex,  $\frac{1}{2}\langle 111 \rangle$ , 7-SIA cluster (as representative of one-dimensionally gliding clusters) in pure Fe and in Fe–1.0 at. % Cu.

### 1. Vibrational modes of the self-interstitial atom

According to Dederichs and Lehmann,<sup>32</sup> the dominant resonant modes for split self-interstitials in metals are librational (both atoms vibrating in opposite phase in the direction perpendicular to the interstitial axis), responsible for changing the orientation of the interstitial axis, and axial (both atoms vibrating in phase in the direction of the interstitial axis), responsible for one-dimensional translation. These modes give rise to an attempt frequency in the direction of the escape coordinate (toward the dividing surface of two different stable states, i.e., the saddle point configuration) and can be calculated using crystal vibrations theory in the harmonic approximation.<sup>33</sup>

From Eq. (6) we have calculated the attempt frequencies, as well as the static energy barriers, of the interstitial in pure Fe and several different Cu-SIA configurations (Table II) for the  $\langle 111 \rangle$ -to- $\langle 110 \rangle$  rotation step, required to evaluate  $I_{\text{Fe}}^2/I_{\text{FeCu}}^2$ . Interestingly, however, we have not found significant differences among any of the structures studied. The attempt frequencies are in all cases very close to 10.0 THz, indicating that the force constants along the  $\langle 111 \rangle$ -to- $\langle 110 \rangle$  reaction coordinate are dominated by the interstitial, rather than by the Cu atom. This means that the  $\Gamma_{0,\text{Fe}}^{\langle 111 \rangle - \langle 110 \rangle} / \Gamma_{0,\text{FeCu}}^{\langle 111 \rangle - \langle 110 \rangle}$  quotient in the denominator of Eq. (5) is very close to unity. Likewise, the static energy barriers do not differ significantly, which means that the exponential term in the denominator of Eq. (5) is close to 1 as well.

The picture is somewhat different for the case of  $\langle 111 \rangle$  dumbbell and crowdion migration. The  $\langle 111 \rangle$  crowdion is an intermediate, metastable step between the  $\langle 111 \rangle$  dumbbell and the saddle point along the  $\langle 111 \rangle$  migration coordinate. The energy difference between either of these states is very small ( $\sim 0.01$  eV), meaning that vibrational excursions from one state to another at moderate temperatures occur frequently (making it rather difficult to define when the defect resides in one state or the other). This makes the interstitial develop a soft (low-frequency) vibrational mode that gives rise to diffusion. For the case of the  $\langle 111 \rangle$  translation in pure Fe we obtained an attempt frequency of  $2.03 \times 10^{12}$  Hz and a static migration energy of 0.037 eV, whereas for the case of the  $\langle 111 \rangle$  translation with a Cu forming part of the crowdion chain we obtained values of  $1.24 \times 10^{12}$  Hz and 0.045 eV, respectively. This difference in energy, at the temperatures of our study, renders the exponential term in the numerator of

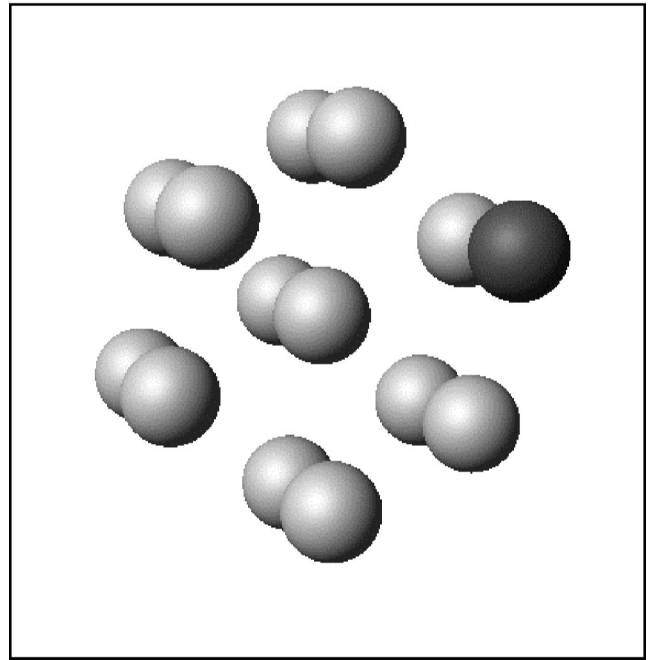


FIG. 6. Atomic representation obtained by MD of a 7-SIA, hexagonal cluster, used for vibrational entropy calculations. The darker atom is the one assumed to generate a kink pair by jumping one Burgers vector distance outside the habit plane.

Eq. (5) virtually 1. The attempt frequency in pure Fe is, however, 1.6 times larger than when there is a solute atom involved, in good agreement with the expected value of  $\sim 2.0$ , which substantiates the variance observed in the prefactors calculated by dynamical simulation. (Despite the fact that the value of 2 applies only to 1D diffusion and that this analysis has been made for a single SIA, which bears 3D migration, one-dimensionally gliding SIA clusters move at the atomic level as consequence of  $\langle 111 \rangle$  crowdion jumps. Therefore the single-interstitial analysis can be helpful in explaining the differences observed for 1D clusters.)

The differences in pure Fe and Fe–1.0 at. % Cu are therefore more pronounced regarding the  $\langle 111 \rangle$  jump and account for the quantitative differences observed in the diffusion prefactors of the single SIA.

### 2. Analysis of the vibrational modes of a 7-SIA cluster

For the case of the 7-SIA cluster (*magic number*, hexagonal loop, Fig. 6), we are faced with the problem of establishing the stable and saddle point configurations for Eq. (6). As pointed out in Sec. III, the migration mechanism of a SIA loop is a complex, multistep process that involves kink-pair nucleations at one or more locations in the loop, kink propagation from one or several of these kink-nucleation sites, and kink interactions, all of which can occur in a very interdependent, correlated manner. Thus the problem of defining clear saddle points between each of these states is ill defined and its complexity is beyond the scope of this work. In Sec. III B 1, we demonstrated that the  $\langle 111 \rangle$  jump is the dominant step in the single-interstitial prefactor. Since any cluster larger than  $n=3$  undergoes exclusively 1D migration



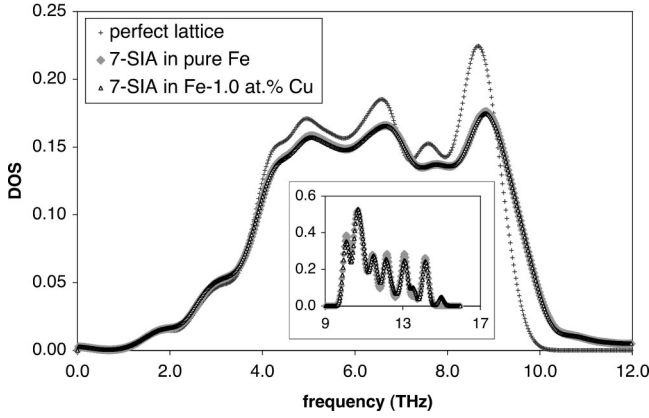


FIG. 7. Phonon density of states of an  $\alpha$ -Fe perfect lattice and Fe and Fe–1.0 at. % Cu lattices containing a 7-SIA cluster. The most significant difference between the perfect lattice and the defect structures is the high-frequency tail (depicted in the inset).

through multiple  $\langle 111 \rangle$  jumps, it is intuitive to believe that the same conclusions drawn there apply in this case, i.e., low-frequency modes dominate the differences between diffusion in pure Fe and Fe–1.0 at. % Cu. However, the cluster nature of the defect may introduce collective effects that cannot be disregarded with such a simple reasoning and a specific study of cluster vibrational properties has been undertaken.

For the sake of simplicity, we have studied the contribution to the overall prefactor of a single kink-pair nucleation at one of the corners of the hexagon, which in this case corresponds to having one of the constituent SIA's undergo a single  $\langle 111 \rangle$  jump outside the equilibrium habit plane of the cluster (atom highlighted in Fig. 6). We are interested in understanding the unique features introduced by the SIA cluster and, in the Fe-Cu case, the Cu atoms. The analysis has been carried out in a  $7a_0 \times 7a_0 \times 7a_0$  box containing the interstitial cluster (693 atoms), which yields 2079 normal vibration modes. This information can be conveniently summarized by the phonon density of states (DOS), which gives the number of modes of oscillation having a frequency lying in the interval  $[\omega, \omega + d\omega]$ :

$$g(\omega) = \sum_{\alpha=1}^{3N} \delta(\omega - \omega_{\alpha}), \quad (7)$$

where the  $\omega_{\alpha}$ 's are the normal vibration (angular) frequencies of the defect crystal ( $2\pi\nu_{\alpha}$ ). The DOS for the defect crystals in pure Fe and in the Fe-Cu alloy, at the SIA cluster equilibrium configuration, are shown in Fig. 7. The DOS for the  $\alpha$ -Fe perfect lattice is also shown for comparison (the Fe–1.0 at. % Cu perfect lattice is virtually identical). Comparing the DOS of the defect lattices with the perfect lattice DOS, among other features, we notice the presence of a number of localized modes grouped in a high-frequency tail. The two defect DOS are almost identical, an expected result given that the difference between both crystals is merely a 1%-different chemical composition. The DOS curves are in good agreement with theoretical and experimental

results,<sup>34,35</sup> despite the artificial fine structure in the band modes due to finite-size effects.

Making use of the data in Fig. 7 and the corresponding data for the saddle point configurations in each case, we have computed using Eq. (6), the attempt frequency corresponding to the aforementioned double-kink nucleation mechanism, and found  $\Gamma_0 = 5.78 \times 10^{12}$  Hz in pure Fe versus  $2.41 \times 10^{12}$  Hz in Fe–1.0 at. % Cu, i.e.,  $\Gamma_0^{\text{Fe}}/\Gamma_0^{\text{Fe-Cu}} = 2.4$ , in very good agreement with the simulation results. Nonetheless, if we break the phonon spectra of both materials into a low- and a high-frequency part, then

$$\Gamma_0 = \frac{\prod_{i=1}^n \omega_i \left| \prod_{i=n}^m \omega_j \right|_{\omega > \omega_c}}{\prod_{j=1}^t \omega'_j \left| \prod_{j=1}^t \omega'_j \right|_{\omega > \omega_c}} = \Omega_{\omega < \omega_c} \Omega_{\omega > \omega_c}, \quad (8)$$

where  $\omega_c = 6.5 \times 10^{13}$  rad s<sup>-1</sup> ( $\sim 10$  THz, beyond the band modes of the perfect lattice) and  $n + m = 3N$  and  $l + t = 3N - 1$ , and calculate the quotient

$$\frac{\Gamma_0^{\text{Fe}}}{\Gamma_0^{\text{Fe-Cu}}} = \frac{\Omega_{\omega < \omega_c}^{\text{Fe}} \Omega_{\omega > \omega_c}^{\text{Fe}}}{\Omega_{\omega < \omega_c}^{\text{Fe-Cu}} \Omega_{\omega > \omega_c}^{\text{Fe-Cu}}} = K_{\omega < \omega_c} K_{\omega > \omega_c} \quad (9)$$

we obtain for  $K_{\omega < \omega_c}$  a value of 2.24, whereas  $K_{\omega > \omega_c} = 1.07$ . The inset in Fig. 7 shows the normalized DOS for frequencies  $\geq 9.0$  THz. The spectra are composed of six clearly distinguishable peaks and are very similar in both materials. The peaks generally have a sevenfold degeneracy corresponding to modes with identical frequencies localized around each one of the interstitial atoms forming part of the cluster. This degeneracy is slightly altered by the symmetry-breaking structure of the cluster and other external factors, including perhaps Cu solute atoms (the reason why the peaks are not narrower—in theory they ought to be  $\delta$  functions<sup>34</sup>). However, the curves confirm that the relative importance of each peak is approximately the same in both materials, resulting in no appreciable differences.

This leads to the conclusion that the main differences between both cases are caused by variations introduced by Cu atoms in the distribution of normal modes in the resonant range and that it is these variations that account for the prefactor discrepancy in both materials. To get a better insight into this solute effect we have obtained the local DOS, which, similar to Eq. (7), gives the number of modes in the frequency interval  $[\omega, \omega + d\omega]$ , projected on atom  $i$  along direction  $\mathbf{r}$ :

$$g_{\alpha}^i(\omega) = \sum_{\alpha=1}^{3N} |\boldsymbol{\varepsilon}_{\alpha}^i \cdot \mathbf{r}|^2 \delta(\omega - \omega_{\alpha}), \quad (10)$$

where  $\boldsymbol{\varepsilon}^i$  is the polarization vector associated to atom  $i$ . The local DOS for the equilibrium and saddle point configurations, projected on the corner atom of the 7-SIA cluster (highlighted in Fig. 6) along the  $\langle 111 \rangle$  direction, are shown for pure Fe and Fe-Cu in Fig. 8. Analyzing the differences between the vibrational spectra in the equilibrium and saddle

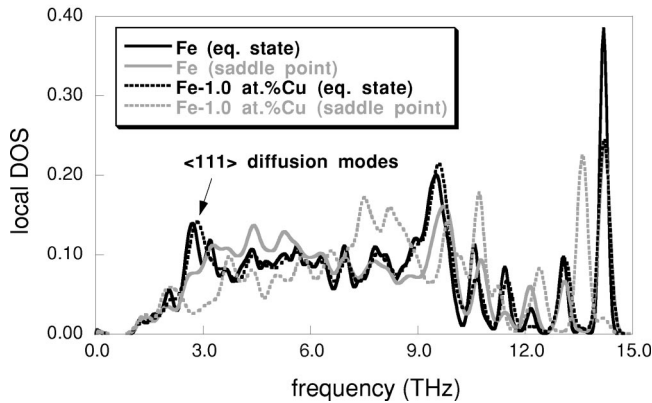


FIG. 8. Local phonon density of states projected on one of the corner atoms of the 7-SIA cluster (darker atom in Fig. 6), along the diffusion  $\langle 111 \rangle$  direction, in pure Fe and in Fe-1.0 at. % Cu. The low-energy modes that give rise to diffusion are pointed out in the graph.

point configurations, we are able to identify the modes along the reaction coordinate, i.e., the resonant mode that gives rise to diffusion and its corresponding high-frequency counterpart,<sup>34</sup> as they are absent or significantly attenuated in the saddle point spectrum. These modes are located for both materials at frequencies  $\sim 2.7$  THz and  $\sim 11.4$  THz, respectively. However, while the curves for the cluster equilibrium configuration are quite similar in both cases, at the saddle point both results differ significantly. Particularly, in the frequency range that contains the diffusion modes, the local DOS for Fe-Cu is considerably softer than the one for pure Fe. Here Cu atoms positioned in planes perpendicular to the migration coordinate possibly have a small effect, relaxing the large strains generated by interstitials diffusing along the  $\langle 111 \rangle$  direction. Although this qualitative explanation suffers from limited statistics and would require a more exhaustive analysis, there is quantitative evidence from the calculations above that Cu atoms in solution result in a decreased vibrational entropy for SIA clusters.

Thus the vibrational analysis confirms that, for small sizes, when the self-interstitial cluster is positioned so that its compressive atomic displacement region overlaps with that of the Cu atoms, rotations from a  $\langle 111 \rangle$  orientation to another are favored, enhancing the 3D character of cluster motion. This, however, results in an overall decreased effective diffusion and a reduced prefactor. On the other hand, for larger interstitial clusters that undergo rapid 1D migration, Cu atoms soften the low-frequency modes that give rise to cluster migration, resulting in a decreased contribution to the diffusion prefactor as well.

#### IV. SUMMARY AND CONCLUSIONS

The effect of oversized substitutional Cu atoms on migrating SIA's and small SIA clusters is to change the configuration-dependent energies as a result of atomic displacement field interactions. The resulting effect on diffusional properties is twofold. First, the altered cluster configuration-dependent energies result in an enhanced rota-

tion between  $\langle 110 \rangle$  and  $\langle 111 \rangle$  orientations (for  $I_1$ ) and between different  $\langle 111 \rangle$  directions (for  $I_1$ ,  $I_2$ , and  $I_3$ ) and a decreased activation energy for migration. Second, they also result in shorter sets of correlated  $\langle 111 \rangle$  jump sequences and a decreased diffusion prefactor. The combination of these augmented rotation probabilities and reduced one-dimensional jump sequences effectively increases the 3D character of SIA and small SIA cluster diffusion. Nonetheless, while the change in the diffusion parameters is relatively slight, the enhancement of the three-dimensional character of the small SIA cluster migration may be quite relevant to the microstructural evolution of irradiated  $\alpha$ -Fe and  $\alpha$ -Fe-based dilute alloys.

For one-dimensionally gliding loops ( $n \geq 3$ ) no variation in the migration energy is observed due to the absence of changes in the orientation of the Burgers vector of the loops. Moreover, the interaction between the atomic displacement fields of a  $\frac{1}{2}\langle 111 \rangle$  interstitial cluster and a Cu solute atom acts as an obstacle for 1D motion, effectively shortening  $\langle 111 \rangle$  translation trajectories, and again results in a decreased diffusion prefactor.

Based on these phenomena, we have derived generic power laws for  $D_0$  and  $E_m$  that capture all the underlying physics of the interstitial-cluster diffusion processes for a given number of SIA's. In summary, we propose a data table and a set of simple expressions to obtain the diffusion parameters of self-interstitial clusters in pure Fe and in a Fe-1.0 at. % Cu alloy as a function of cluster size. These parameters can now be used in longer-range Monte Carlo or rate theory models and represent a substantial improvement over the constant 0.1 eV value for the migration energy and the classical  $1/n$  dependence for the preexponential factors used in several previous studies.<sup>9,30</sup> The calculated formulas for pure  $\alpha$ -Fe are

$$E_m(n) = 0.06 + 0.07n^{-1.3} \text{ (eV)},$$

$$D_0(n) = 8.98 \times 10^{-3} n^{-0.61} \text{ (cm}^2 \text{ s}^{-1}\text{)}$$

for one-dimensionally gliding clusters

and in Fe-1.0 at. % Cu:

$$E_m(n) = 0.05 + 0.04n^{-3.1} \text{ (eV)},$$

$$D_0(n) = 5.07 \times 10^{-3} n^{-0.74} \text{ (cm}^2 \text{ s}^{-1}\text{)}$$

for one-dimensionally gliding clusters.

For the preexponential factor of small clusters migrating three dimensionally we propose the data in Table I.

#### ACKNOWLEDGMENTS

Fruitful discussions with Dr. P. Derlet and Dr. M. J. Canturla are acknowledged. This work has been performed under the auspices of the U.S. Department of Energy and Lawrence Livermore National Laboratory under Contract No. W-7405-Eng-48. Two of the authors (J.M. and J.M.P.) would like to acknowledge financial support from the VENUS project within the CSN-UNESA PCI under Contract No. P000531499. G.R.O. acknowledges support from the U.S. National Regulatory Commission under Contract No. NRC-04-94-049.

- <sup>1</sup>D. J. Bacon, A. F. Calder, F. Gao, V. G. Kapinos, and S. J. Wooding, *Nucl. Instrum. Methods Phys. Res. B* **102**, 37 (1995).
- <sup>2</sup>W. J. Phythian, R. E. Stoller, A. J. E. Foreman, A. F. Calder, and D. J. Bacon, *J. Nucl. Mater.* **223**, 245 (1995).
- <sup>3</sup>R. E. Stoller, *J. Nucl. Mater.* **237**, 999 (1996).
- <sup>4</sup>D. Grasse and B. von Guerard, *J. Nucl. Mater.* **120**, 304 (1984).
- <sup>5</sup>R. Rauch, J. Peisl, and A. Schmalzbauer, *J. Nucl. Mater.* **168**, 101 (1989).
- <sup>6</sup>I. M. Robertson, M. L. Jenkins, and C. A. English, *J. Nucl. Mater.* **108–109**, 209 (1982).
- <sup>7</sup>M. Kiritani, *J. Nucl. Mater.* **216**, 220 (1994).
- <sup>8</sup>B. D. Wirth, G. R. Odette, D. Maroudas, and G. E. Lucas, *J. Nucl. Mater.* **276**, 33 (2000).
- <sup>9</sup>N. Soneda and T. Diaz de la Rubia, *Philos. Mag. A* **78**, 995 (1998).
- <sup>10</sup>Y. N. Osetsky, D. J. Bacon, and A. Serra, *Philos. Mag. Lett.* **79**, 273 (1999).
- <sup>11</sup>H. Trinkaus, B. N. Singh, and A. J. E. Foreman, *J. Nucl. Mater.* **199**, 1 (1993).
- <sup>12</sup>B. N. Singh and A. J. E. Foreman, *Philos. Mag. A* **66**, 975 (1992).
- <sup>13</sup>C. H. Woo and B. N. Singh, *Philos. Mag. A* **65**, 889 (1992).
- <sup>14</sup>M. L. Jenkins, M. A. Kirk, and W. J. Phythian, *J. Nucl. Mater.* **205**, 16 (1993).
- <sup>15</sup>R. J. DiMelfi, D. E. Alexander, and L. E. Rehn, *J. Nucl. Mater.* **252**, 171 (1998).
- <sup>16</sup>P. T. Heald, *Philos. Mag.* **31**, 551 (1975).
- <sup>17</sup>N. Soneda and T. Diaz de la Rubia, *Philos. Mag. A* **81**, 331 (2001).
- <sup>18</sup>A. V. Barashev, Y. N. Osetsky, and D. J. Bacon, *Philos. Mag. A* **80**, 2709 (2000).
- <sup>19</sup>G. R. Odette and B. D. Wirth, *J. Nucl. Mater.* **251**, 157 (1997).
- <sup>20</sup>M. K. Miller, P. Pareige, and M. G. Burke, *Mater. Charact.* **44**, 235 (2000).
- <sup>21</sup>G. R. Odette, B. D. Wirth, D. J. Bacon, and N. M. Ghoniem, *MRS Bull.* **26** (3), 176 (2001).
- <sup>22</sup>J. M. Perlado, J. Marian, D. Lodi, and T. Diaz de la Rubia, in *Multiscale Phenomena in Materials—Experiments and Modeling*, edited by B. Devincere, D. H. Lassila, R. Phillips, and I. M. Robertson, *MRS Symposia Proceedings No. 578* (Materials Research Society, Warrendale, PA, 2000), p. 243.
- <sup>23</sup>J. Marian, B. D. Wirth, J. M. Perlado, G. R. Odette, and T. Diaz de la Rubia, in *Microstructural Processes in Irradiated Materials*, edited by G. E. Lucas, L. Snead, M. A. Kirk, and R. G. Elliman, *MRS Symposia Proceedings No. 650* (Materials Research Society, Warrendale, PA, 2000), p. R6.9.
- <sup>24</sup>J. Marian, B. D. Wirth, J. M. Perlado, G. R. Odette, and T. Diaz de la Rubia, *Phys. Rev. B* **64**, 094303 (2001).
- <sup>25</sup>T. Diaz de la Rubia and M. W. Guinan, *Mater. Res. Forum* **174**, 151 (1990).
- <sup>26</sup>G. J. Ackland, D. J. Bacon, A. F. Calder, and T. Harry, *Philos. Mag. A* **75**, 713 (1998).
- <sup>27</sup>M. W. Guinan, R. N. Stuart, and R. J. Borg, *Phys. Rev. B* **15**, 699 (1977).
- <sup>28</sup>B. D. Wirth, G. R. Odette, D. Maroudas, and G. E. Lucas, *J. Nucl. Mater.* **244**, 185 (1997).
- <sup>29</sup>P. Shewmon, *Diffusion in Solids*, 2nd ed. (Minerals, Metals and Materials Society, Warrendale, PA, 1989), p. 109.
- <sup>30</sup>M. J. Caturla, N. Soneda, E. Alonso, B. D. Wirth, T. Diaz de la Rubia, and J. M. Perlado, *J. Nucl. Mater.* **276**, 13 (2000).
- <sup>31</sup>J. P. Hirth and J. Lothe, *Theory of Dislocations*, 2nd ed. (Krieger, Dordrecht, 1982), p. 531.
- <sup>32</sup>P. H. Dederichs and C. Lehmann, *Phys. Rev. Lett.* **31**, 1130 (1973).
- <sup>33</sup>W. M. Franklin, in *Diffusion in Solids: Recent Developments*, edited by A. S. Nowick and J. J. Burton (Academic, New York, 1975), Chap. 1.
- <sup>34</sup>P. H. Dederichs and R. Zeller, *Point Defects in Metals II*, Springer Tracts in Modern Physics, Vol. 87 (Springer-Verlag, New York, 1980).
- <sup>35</sup>H. K. Mao, J. Xu, V. V. Struzkhin, J. Shu, R. J. Hemley, W. Sturhahn, M. Y. Hu, E. E. Alp, L. Vocadlo, D. Alfê, G. D. Price, M. J. Gillan, M. Schwoerer-Böhning, D. Häusermann, P. Eng, G. Shen, H. Giefers, R. Lübbbers, and G. Wortmann, *Science* **292**, 914 (2001).